Atomistic phenomena in dense fluid shock waves

Author(s):
Schlamp, Stefan; Hathorn, Bryan C.

Publication date:
2008-05

Permanent link:
https://doi.org/10.3929/ethz-a-005708030

Originally published in:
Shock Waves 17(6), https://doi.org/10.1007/s00193-008-0121-6

Atomistic phenomena in dense fluid shock waves

Stefan Schlamp[*] Bryan C. Hathorn[†]

January 10, 2008

Abstract

The shock structure problem is one of the classical problems of fluid mechanics and at least for non–reacting dilute gases it has been considered essentially solved. Here we present a few recent findings, to show that this is not the case. There are still new physical effects to be discovered provided that the numerical technique is general enough to not rule them out a priori. While the results have been obtained for dense fluids, some of the effects might also be observable for shocks in dilute gases.

Key words: shock structure, anisotropy, molecular chaos, shock thickness, asymmetry factor

1 Introduction

The shock structure problem belongs to the classical problems in fluid mechanics. Attempts to derive the shock thickness trace back well over 100 years [1–3]. The glory days were probably the 1950's and 60's when experimental facilities and measurement techniques became available, which allowed the experimental validation of the various theories and results that had been proposed and obtained by then. A second wave of interest started

[*]ETH Zürich, Institute of Fluid Dynamics, Sonneggstr. 3, 8092 Zürich (Switzerland)

[†]Oak Ridge National Laboratories, Division of Computer Science and Mathematics, Oak Ridge, TN 37831 (USA)

in the 1960's when computational simulations on an atomistic level became feasible. The breakthrough development was that of the Direct Simulation Monte Carlo (DSMC) technique. Bird, who first introduced DSMC [4], was also the first to apply this technique to the shock wave problem [5]. It was not clear initially whether the procedure was actually solving the Boltzmann equation until Bird himself [6] proved this. DSMC was applied numerous times to the shock structure problem in the following years and today is the work horse in rarefied gas dynamics.

Molecular dynamics (MD) is conceptually much simpler than DSMC, and was consequently proposed before DSMC [7]. But because it is computationally much more expensive, especially at low densities, the first shock wave simulations lagged those for DSMC. Hoover [8] and Holian [9] can be seen as pioneers in applying MD to the shock structure problem.

Because of the incredible wealth of theoretical, experimental, and numerical work in existence on the subject, it is impossible to give a fair and balanced overview here. Suffice it to say that a huge body of knowledge exists, but that the focus in the meantime has shifted away from the "classical" shock structure problem. Instead, shocks in chemically reacting fluids, shocks in solids with grain boundaries, etc. have taken center–stage. This is due to the fact that for all practical purposes the "classical" shock structure problem is considered solved – not in the sense of having a closed–form analytical solution (should one exist), but at least numerically. This is true in as far as the Boltzmann equation now can be solved to arbitrary accuracy. One is content to know that the existing macroscopic governing equations are not applicable for this problem, but since one can use DSMC in those cases or in those regions, a further advancement of the theory seems less important. In any case, agreement between simulations and experiments is very good, and any remaining discrepancies are not significant for engineering purposes.

Then there are a few impediments to someone interested in this problem: the high entry barrier to the field (like in turbulence modeling, but in contrast to those in an emerging specialty), negligible funding for such fundamental research, and the prospect of only being able to make minute quantitative improvements to existing formulations. In fact, the original purpose of the work presented here was to provide validation data for other, more efficient numerical techniques. It was assumed that all physical effects relevant to the shock wave problem had been found and reported on. The data analysis showing some unanticipated effects (in particular, Secs. 4–6) were primarily meant to verify the proper behavior of the code and convergence of the

simulations. The objective of this paper is then less to document in detail each one of the findings (yet they are described with some background for their understanding), but to show that even classical problems might not be as fully explored as they appear.

Some of the results have been published in more detail elsewhere and the reader is kindly asked to consult the references for a more complete description, theoretical background, discussion of results etc. Sec. 2 introduces the numerical technique and the particular setup used. Sec. 3 gives a brief review of the macroscopic shock structure. Each of Secs. 4 through 7 will then discuss one phenomenon which has only recently come to light (see Refs. [10–12], respectively, for more details). These are all aspect of a broader research project carried out over the last several years at ETH Zurich [13]. Here we only report on some of the results for the shock wave in dense nitrogen, but the same results (where applicable) have been observed in argon.

2 Numerical setup

Like DSMC, MD is particle–based and does not directly solve a macroscopic governing equation (e.g. Navier–Stokes). But unlike DSMC, MD simulates the movement of each real particle, i.e., there is no distinction between real and computational particles.

While DSMC can be shown to solve the Boltzmann equation, MD solves no macro- or microscopic governing equation for a fluid; only the Newtonian equations of motion are solved. It hence does not require any a priori assumptions or knowledge about the fluid, e.g. an equation of state and the transport coefficients (as required by macroscopic governing equations) or a collision model (as required by DSMC).

The forces between pairs of particles are calculated based on some potential function, the choice of which is the only form of modeling required. These range from hard–sphere models over generic potentials to many–parameter functions, which reproduce the thermodynamic and physical properties of fluids and solids quantitatively over a wide range of densities and temperatures. The computational cost of calculating forces between all possible particle pairs in the domain scales as N^2, but this growth can be made linear by a finite cut–off radius beyond which molecules are not considered for the force calculation.

MD was first proposed by Alder and Wainwright in the 1950s [7]. It does not make the assumptions underlying the Boltzmann equation and is thus well–suited even for high densities and can even be used for simulations of solids. In fact, MD is prohibitively expensive for low densities. Hoover [8] and Holian et al. [9], for example, use MD to simulate shock waves in dense monatomic gases. They find that the discrepancies between the Navier–Stokes and the MD results is smaller than for dilute gases. Tsai and Trevino [14] perform MD simulations of shock waves in liquids.

MD has been applied repeatedly for this fluid mechanical problem (e.g. [9, 15, 16]). These works focus on the steady–state profile. A setup similar to the one used here, namely the creation of the shock by an impulsively accelerated piston, has also been studied in Refs. [17–19]. These authors obtain temporally resolved data for the formation of the steady state profile from an initially quiescent fluid. All of the above only consider monatomic gases, i.e., do not consider rotational degrees of freedom. Steady–state profiles for a shock in dilute nitrogen has been obtained using a hybrid method (MD + Direct Simulation Monte Carlo) by Tokumaso and Matsumoto [20]. In the present work, for the first time, the shock structure of a diatomic dense fluid is considered.

All results reported in the subsequent section are based on the same set of molecular dynamics simulations. The numerical setup is the same discussed in detail in Ref. [11]. Only the most essential parameters are reproduced here. The molecular dynamics code used is a modified version of *Moldy* [21]. The computational domain is a cuboid with dimensions $L_x \times L_y \times L_z = 252 \times 237.9 \times 237.9$ $\mathring{A}^3$, where a layer of 15.86 $\mathring{A}$ thickness on either side (in x–direction) is occupied by a piston and by a stationary wall.

$100,000$ nitrogen molecules are randomly distributed within the fluid portion of the domain and given random initial velocities and rotation rates drawn from a Maxwell–Boltzmann distribution. The rigid nitrogen molecule is modeled by a two–center Lennard–Jones (6,12) potential with the parameters as given in Ref. [22], but without the five point–charges. The mean distance between molecules is $\delta = n^{-1/3} = 5$ $\mathring{A}$ initially, where n denotes the number density. The mean free path (based on its dilute gas definition and using $2\sigma_{LJ}$ as diameter) is $\mathcal{O}(1$ $\mathring{A})$.

The system is equilibrated for 2 ps, where the molecular velocities and rotation rates are rescaled periodically to correspond to the desired initial temperature of 300 K. The shock wave is created by impulsively accelerating the left wall (piston) to a velocity of $u_p = 1,000$ m/s. The system state

is saved every 0.05 ps. 10 ensembles with perturbed initial conditions are simulated. The averaged shock structure is obtained by averaging over all ensembles and over all time steps where the shock wave is at least 50 $\mathring{A}$ from either wall.

3 Macroscopic shock structure

The shock thickness Λ based on the maximum density gradient is defined as

$$\Lambda = \frac{\Delta\rho}{\left.\frac{d\rho}{dx}\right|_{max}}, \tag{1}$$

where $\Delta\rho$ denotes the density jump across the shock. The denominator is the largest spatial density gradient within the shock waves. Λ thus represents the distance over which the maximum gradient would have to be maintained in order to achieve the same density jump.

For dilute gases Λ tends to infinity for weak shocks, but is usually in the range between 2 to 4 mean–free paths for $M > 1.5$ with a slightly increasing tendency for large Mach numbers [23]. For a given Mach number, the shock thickness increases slightly (relative to the mean–free path) with the density [24].

Over this short distance, the fluid state changes significantly so that it is immediately obvious that the continuum hypothesis is not applicable within the shock. Fig. 1 shows a particular example for a shock in dense nitrogen. Yet the dilute shock structure is very similar when properly scaling the horizontal axis. All quantities have been nondimensionalized by the pre– and post–shock properties,

$$\tilde{q} = \frac{q - q_1}{q_2 - q_1}, \tag{2}$$

where the subscripts 1 and 2 denote the pre– and post–shock state, respectively. q could refer to the density, velocity, temperature, etc. Hence, zero corresponds to the pre–shock state and unity is the post–shock value. The origin of the spatial coordinate system has been chosen such that $x = 0$ corresponds to the location where $\tilde{\rho} = 0.5$.

The breakdown of the local thermodynamic equilibrium (LTE) hypothesis is evident from the fact that the equi–partition of energy theorem is violated. It states that the energy is divided equally between all available degrees of

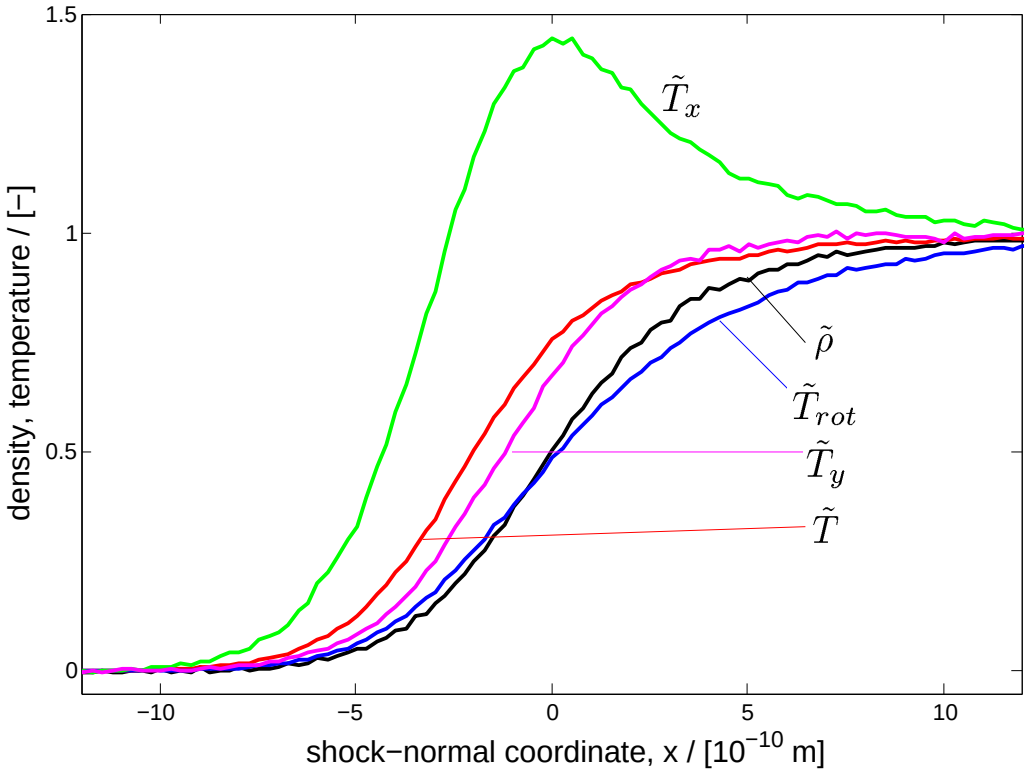

Figure 1: Shock structure ($M = 3.56$) in dense nitrogen ($T_1 = 300$ K, $\rho_1 = 370.9$ kg/m^3, $T_2 = 978$ K, $\rho_2 = 741$ kg/m^3, $\Delta u = 985$ m/s). The velocity profile (not shown for clarity) is similar to that of $\tilde{T}_y$.

freedom (our simulations neglect quantum mechanical effects). This would require that the rotational temperature is equal to the translational temperature, which is not the case in a shock wave. Furthermore, Fig. 1 also shows that not even the three translational degrees of freedom are equally excited: The translational temperature based solely on the shock–normal velocity component ($\tilde{T}_x$) deviates from that based on the shock–parallel motion ($\tilde{T}_y$). Note in particular the well–known temperature overshoot of the shock–normal temperature component, whose magnitude depends on the Mach number and the ratio of specific heats. This overshoot was first predicted theoretically [25, 26], but later confirmed experimentally (Ref. [27] is a more recent example).

Our results for dense fluids indicate that the asymmetry parameter [28]

(Ref. [29] uses a slightly different definition)

$$Q = \frac{\int_0^\infty (\rho - \rho_1) dx}{\int_{-\infty}^0 (\rho_2 - \rho) dx}. \tag{3}$$

is less than unity whereas it is found to be greater than unity in dilute gases for comparable Mach numbers [28, 29].

Not surprisingly, the Navier–Stokes equations do not even reproduce the shock thickness well for $M_s > 2$ [30]. But there certainly exist more refined governing equations, which yield satisfactory agreement, at least for dilute gases. But instead of dwelling on subtle quantitative discrepancies between various techniques, Secs. 4 through 7 will address features, which none of the existing techniques is able to capture at all.

4 Anisotropic molecular orientations

Intuitively, due to the frequent collisions, one would assume that the angular orientation of the molecules is random. In fact, in the context of dilute fluids, this follows almost directly: In dilute fluids, the distance between molecules is much larger than the size of a molecule. The molecules hence only interact during collision events, which are very short compared to the time spent between collisions. The orientations of colliding molecules are randomized by the collision. But since there are no interactions between the collision events, there is no mechanism which could produce an anisotropic orientation of the molecules. For dense fluids, the situation is different. The trajectory of a molecule is not governed by isolated binary collision events, but rather by a continuous interaction with multiple neighboring molecules. If their distribution is inhomogeneous (e.g. by means of a strong density gradient), then this could produce an anisotropy.

Molecules near a phase boundary have an alignment tendency, e.g. water molecules very close to the surface [31], polar [32] and non–polar [33] molecules at the water/air interface in a Langmuir monolayer, or surfactant molecules in a liquid colloid (micelle) [34]. The alignment of liquid crystals in the nematic phase can be controlled by applying an electric field [35].

Subsequently, only homo–nuclear diatomic molecules are considered, but the terminology is easily extended to a more general case. Let the orientation

angle θ be the angle between the x–axis and the inter–nuclear axis. Because the nitrogen molecule is symmetric, θ is mapped to the range $0 \ldots \pi/2$ without loss of generality. $\theta = 0$ then means that the molecule is aligned along the shock normal vector, while $\theta = \pi/2$ for a molecule, whose axis is parallel to the plane of the shock wave. Similarly, ϕ $(0 \ldots \pi/2)$ denotes the angle between the x–axis and the angular momentum vector (i.e., the instantaneous "rotation axis"). For a linear molecule, the angular momentum has to be perpendicular to the molecule's axis. This represents the constraint

$$0 \leq \pi/2 - \phi \leq \theta. \tag{4}$$

Purely random orientations of the molecules and the axes of rotation would yield distributions $f_\theta = \sin\theta$ and $f_\phi = \sin\phi$, merely reflecting the different solid angles. Deviations are then evident by non–zero values of $\tilde{f}_\theta = (f_\theta - \sin\theta)/\sin\theta$ and $\tilde{f}_\phi = (f_\phi - \sin\phi)/\sin\phi$. These are the relative over– or underpopulations of a certain value for θ or ϕ.

Fig. 2(a) & (b) shows these deviations across the shock wave. The horizontal axis is the shock–normal coordinate, the vertical axes represent θ and ϕ. The color coding refers to the over– (red) or under–population (blue) as given by $\tilde{f}_\theta$ and $\tilde{f}_\phi$.

It can be seen that θ and ϕ are distributed randomly upstream and downstream of the shock. Within the shock wave ($|x/\Lambda| \leq 1$), large θ are overpopulated, while small θ are underpopulated. The trend is weak (at least for these fluid conditions), but clearly visible above the background noise. The opposite behavior is observed for the angular momenta. Within the shock, small values of ϕ are overpopulated, large ϕ are underpopulated. But the effect for the angular momentum orientation is weaker.

The anisotropy of ϕ requires an opposite (in sign but not in magnitude) anisotropy of ϕ, and vice versa: The overpopulation of small θ does not mean that molecules "freeze" in a particular orientation. On the contrary, the rotational temperature (and thus the mean rotation rate) increases continuously across the shock wave. Consider the limiting case where each molecule has $\theta = 0$. Then, because of Eq. 4, each molecule would also necessarily have $\phi = \pi/2$. But even for a smaller anisotropy of θ, Eq. 4 leads to an opposite effect for ϕ. This argument implies a cause and effect relationship, i.e., that the anisotropy of θ causes the anisotropy of ϕ. This is not the case. In reality both effects are simply coupled through Eq. 4.

But one might wonder why $\tilde{f}_\theta$ deviates further from zero than $\tilde{f}_\phi$. This

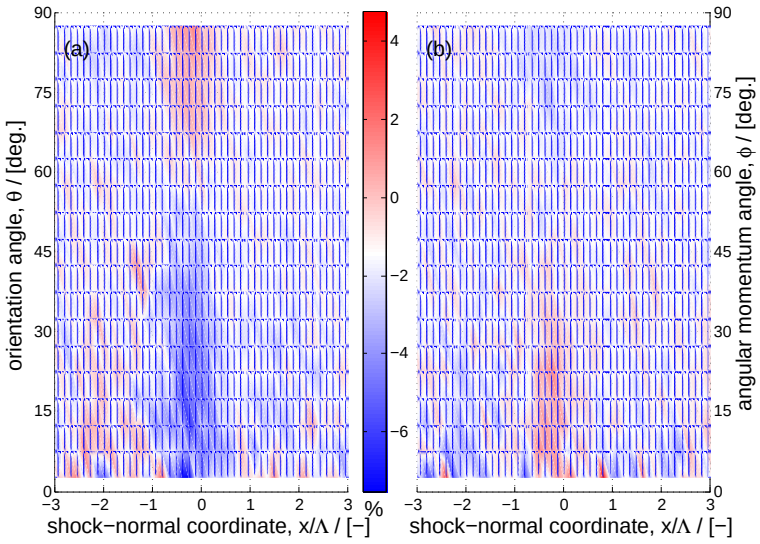

Figure 2: Orientation angle distributions across shock wave; (a, left) population enhancement of orientation angles relative to a purely random distribution; (b, right) the same, but for the orientation of the angular momentum vector. Flow is from left to right. The horizontal scale has been nondimensionalized by the shock wave thickness $\Lambda = 7.5$ $\mathring{A}$. The shock conditions are the same as in 1.

can be understood by considering that the effect is due to the interaction with inhomogeneously distributed molecules in the vicinity. It is thus a function of the location of the two nitrogen atoms (i.e., the orientation), but not on their velocity vector (i.e., the angular momentum vector). The angular momentum only becomes significant because it determines the location of the atoms subsequently.

We have proposed [10] a nondimensional parameter governing the magnitude of the anisotropy, which includes the elongation of the molecule, the magnitude of the density gradient, the density, and the curvature of the potential function between molecules. Additional simulations with different flow conditions are required to confirm this scaling.

A posteriori (see Ref. [10] for a proposed mechanism), it seems obvious that such an alignment effect could (and should) exist and one wonders why it has not been observed before. One must note that all of the following

conditions must be met to observe the phenomenon: a) the molecular model must be non–spherical; b) it is a dense gas effect. Simulations in dilute gases will not produce an alignment; c) realistic (i.e., smooth) interaction potentials are required. Simulations of hard–sphere molecules will not produce an alignment; d) the effect is weak. Large sample sizes are required to observe it above the statistical fluctuations; e) one has to look for it.

5 Higher moments of the velocity distribution function

While the previous section addressed a feature which cannot be captured by present theories, this and the next section show that (and by how much) the underlying assumptions of various governing equations are violated. All common macroscopic governing equations of fluid mechanics are derived from the Boltzmann equation. The Euler and the Navier–Stokes equations, for example, are the zeroth and first order series expansions with respect to the Knudsen number (Chapman–Enskog expansion) [36].

In general, the closure problem consists of expressing the heat flux and the stress tensor as a function of the other quantities and their derivatives. The fluctuation theorem [37] provides expressions, which are valid in general, but which can not be calculated. It can be seen as a microscopic version of the second law of thermodynamics. The Green–Kubo relations [38–41] are a simplification of the fluctuation theorem, but are only valid for fluids close to equilibrium [42]. Also, they are not applicable for *flow* simulations. This is, because they do not provide *instantaneous* values for the transport coefficients.

One instead (explicitly or implicitly) makes certain assumptions about the moments of the velocity distribution function above some order. The Euler equations, for example, follow from the Boltzmann equation in the high collision rate limit. In this limit, the molecular velocities follow an equilibrium, i.e., Maxwell–Boltzmann distribution, for which all odd moments are zero. The heat flux is proportional to the skewness (the third central moment) of the velocity distribution function. This is responsible for the non–heatconducting nature of the Euler equations.

The Navier–Stokes equations account for non–zero skewness, but similar assumption for the moments of order four and up are required in their

derivation from the Boltzmann equation. It has to be said, however, that the Fourier law (of heat conduction) and Newtonian behavior are a consequence of the derivation and not an a priori assumption. Higher–order terms of the Chapman–Enskog series are the Burnett and super–Burnett equations, for which the closure problem is shifted to moments of order 5 and 6, respectively [36].

Let $\vec{\xi^i} = (\xi^i, \eta^i, \zeta^i)$ and $\vec{c^i} = (c_x^i, c_y^i, c_z^i)$ be the location and the velocity vector of molecule i in the shock–fixed reference frame, respectively. We define the central moments as follows:

$$\mu_0 = N = \sum_{i=1}^{N} 1 \qquad \mu_{1,\alpha} = \vec{u}_\alpha = \frac{1}{N} \sum_{i=1}^{N} \vec{c^i_\alpha} \qquad \mu_{k>2,\alpha} = \frac{1}{N} \sum_{i=1}^{N} \left(\vec{c^i_\alpha} - \vec{u}_\alpha(\xi^i) \right)^k \tag{5}$$

Greek subscripts denote components of vectors or tensors. Roman subscripts indicate the order of the moment. The moments for $k > 2$ are tensors, but only the diagonal elements are considered here. The sum is over all molecules within a slice $|x - \xi^i| \leq \delta x/2$ parallel to the plane of the shock wave. It can be seen that μ_0 (when divided by the volume) is just the density, and that μ_1 is the velocity vector of the fluid. μ_2 and μ_3 are proportional to the temperature and heat flux, respectively. Note that μ_2 is a vector, whose elements correspond to the directional temperatures mentioned in Sec. 3. Likewise, μ_3 is a tensor, whereas the heat flux is conventionally assumed to be a vector. This simplification requires that the local thermodynamic equilibrium assumption holds, which has already been shown to be violated within a shock.

The third and higher moments are normalized by the respective power of the standard deviation $\sqrt{\mu_{2,\alpha}}$. The fourth and higher even moments are expressed as excess moments, i.e., the value of the moment which a Maxwell–Boltzmann distribution would have is subtracted ($\mu_{4,MB} = 3$, $\mu_{6,MB} = 15$, $\mu_{8,MB} = 105$, $\mu_{10,MB} = 945$). An equilibrium distribution would thus correspond to all excess moments being zero.

Fig. 3 shows the higher central moments of the velocity distribution function across the shock wave. The even moments are plotted in Fig. 3(a), the odd moments in Fig. 3(b). The solid lines are for the direction along the direction of the main flow ($\alpha = x$ in Eq. 5). The dotted lines are for one of the in–plane velocity components ($\alpha = y$ or z in Eq. 5). Upstream and downstream, all excess moments are zero, consistent with a Maxwell–Boltzmann

distribution of a fluid in equilibrium.

The sensitivity to finite sample size effects increases with the order of the moment. The higher noise levels for the higher orders are thus expected. It is still curious that the largest noise–like fluctuations are limited to a section on the cold side of the shock and are not observed for the in–plane directions.

The most counter–intuitive feature in Fig. 3(a) is that the even moments of order four and higher of the velocity distribution function across the shock wave exhibit a sign reversal. They are positive on the cold side of the shock, but slightly negative on the hot side of the shock. This means that the velocity distribution function changes from having fat tails to having slim tails, at least with respect to the molecular velocities along the shock–normal direction. The distribution function for the in–plane velocity components does not have a sign reversal. We do not expect that this is a dense gas effect.

Experimental and numerical data for dilute gases, from which the higher moments can be extracted, is available in the literature, but to the authors' knowledge, the effect has not been reported previously. The location where the higher out–of plane moments first deviate from zero does not depend on the order of the moment, i.e., the trend for the lower moments that the temperature (second moment) changes upstream of the flow velocity (first moment) and the density (zeroth moment) is not continued or it approaches a limit asymptotically (also see Fig. 1). Consider a collection of molecules in a volume. When a single very fast molecule enters the volume, its (relative) influence on the number of molecules or their mean velocity is small. Its effect is strongest felt for the higher moments, since it is those who capture the tail behavior of the velocity distribution function.

The peak magnitude of the moments increases with the order of the moment (note the different scaling of the lines in Fig. 3). This is significant when considering appropriate closure relations for the atomistic governing equations when deriving macroscopic governing equations from them. The influence on the macroscopic quantities will, for most practical purposes, be negligible because the higher moments are predominantly affected by the (few) particles in the tails of the distribution function. The effect could, however, be large for flows in which high kinetic energy collisions play a significant role, such as for chemically reacting flows.

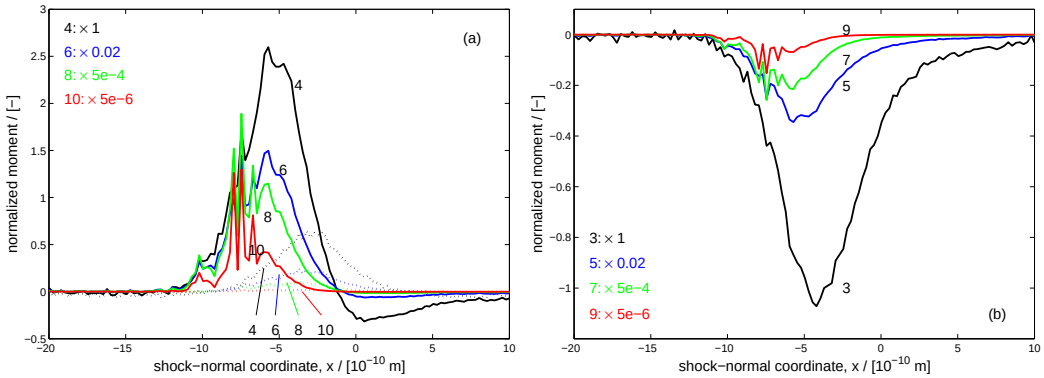

Figure 3: Even (a, left) and odd (b, right) moments of the velocity distribution function for a shock wave in dense nitrogen. The labels indicate the order of the moment. The solid lines are for the molecular velocities in shock–normal direction, the dotted lines for velocities within the shock plane. The odd moments for the shock–parallel velocities are zero (within the measurement uncertainty) and are not shown. The curves are scaled to fit in the same axes. The scaling factors, which have been applied for each order, are shown in each panel.

6 Long–range two–point velocity correlations

The previous section addresses errors in the step between Boltzmann equation and a macroscopic governing equation. Here, we can show that even the assumptions underlying the Boltzmann equation, are not fully satisfied within a shock wave. Grad [43] summarizes these assumptions:

1. point molecules; This is intrinsically implied by writing the distribution function as $f = f(\vec{r}, \ldots)$.

2. complete collisions; There exists a time interval which is large compared to the duration of a collision, yet small compared to the mean time between collisions.

3. slowly varying distribution function; This means that f does not change significantly over the intermediate time scale just mentioned, *i.e.*, $f \approx$ const. over a distance comparable to the size of a molecule (but not necessarily over the mean–free path).

4. molecular chaos; The velocities of two molecules with a distance larger than the range of short–range forces are uncorrelated.

The first three assumptions are satisfied for a dilute gas, but not for a dense fluid (or shock therein). The nice property of the first three assumptions is that their validity can easily be assessed a priori. They only require the knowledge of some length and time scales, which are usually roughly known. This is not so with the last assumption. It has to be evaluated a posteriori, which is what is done here. Note that this evaluation cannot be made after the assumption has been used in the derivation of the governing equation being solved (which could yield a circular argument).

Strictly speaking, it will be shown subsequently that the molecular chaos assumption is violated in a dense fluid shocks. But in dense fluid shocks, the other assumptions do not hold anyway. Yet, our results might not be a dense fluid effect, but might instead be also observable in dilute fluids. Other examples, where the molecular chaos assumption does not hold, include fluids near the liquid–vapor critical–point, where the behavior of the fluid is dominated by long–range correlations, shear flows [44–46], dissipative gases [47], and high–energy heavy–ion collisions [48].

Let $\vec{\Psi}$ be the the kinetic state vector of molecule i,

$$\vec{\Psi}^i = \left(\Psi^i_\perp, \Psi^i_{||}, \Psi^i_\omega\right) \equiv \left(c^i_x, \sqrt{\left(c^i_y\right)^2 + \left(c^i_z\right)^2}, |\vec{\omega}^i|\right). \tag{6}$$

The first component is simple the shock–normal velocity. The second component is the in–plane velocity magnitude. This makes use of the fact that the in–plane directions are interchangeable and that there cannot be a preferred direction. $|\vec{\omega}|$ is the magnitude of the rotation rate vector, i.e., essentially the square root of the rotational kinetic energy. $\vec{\Psi}$ does not have a physical meaning and it does not define the state of a molecule uniquely. It is merely used to simplify the notation.

Let us now define the difference between the state vector of a single molecules and the local average state vector as

$$\tilde{\vec{\Psi}}^i \equiv \vec{\Psi}^i - < \vec{\Psi}^j >, \qquad \forall j \text{ s.t. } |\xi_j - \xi_i| \leq \Delta x/2. \tag{7}$$

where $\Delta x = 1$ $\mathring{A}$ is the spatial resolution. With this notation, the two–point correlation function is

$$R_{\alpha,\beta}(x,r) \equiv \frac{< \tilde{\Psi}^i_\alpha \tilde{\Psi}^j_\beta >}{\sqrt{< \left(\tilde{\Psi}^i_\alpha\right)^2 >< \left(\tilde{\Psi}^i_\beta\right)^2 >}} \quad (8)$$

$$\forall i \text{ s.t. } |\xi^i - x| \leq \frac{1}{2}\Delta x$$

$$\forall j \text{ s.t. } |\xi^j - x| \leq \frac{1}{2}\Delta x$$

$$\text{and} \quad \left|\sqrt{(\eta^j - \eta^i)^2 + (\zeta^j - \zeta^i)^2} - r\right| \leq \frac{1}{2}\Delta r$$

The definition is that of a correlation coefficient, except that the averages in the numerator and the denominator go over different groups of molecules. The numerator is the covariance of the state vector of molecules separated by distance r at the shock–normal coordinate x. The average hence goes over all molecules which are within Δx *and* Δr ($\Delta r = 0.2$ $\mathring{A}$) of each other. The average in the denominator only requires that molecules are within Δx of each other. In practice, the difference between Eq. 8 and the correlation coefficient will be negligible.

The different panels of Fig. 4 show the different components of $R_{\alpha,\beta}(x,r)$ for the $M = 3.56$ shock in dense nitrogen. Note that $R_{\alpha,\beta} = R_{\beta,\alpha}$. The horizontal scale is the shock–normal coordinate normalized by the shock thickness (7.5 $\mathring{A}$). Flow is from left to right, such that the left hand side of each panel corresponds to the cold side of the shock wave. The vertical scale is the radial distance normalized by the Lennard–Jones radius ($\sigma_{LJ,N_2} = 3.318$ $\mathring{A}$) of the nitrogen atom. The strong deviations from zero for the smallest observed spacings (lower edge of the panels) are due to the small number of particle pairs with very small separations and have thus to be interpreted as noise. While R can also be negative, no statistically significant negative values have been observed. The color coding thus only covers positive values.

Upstream and downstream of the shock wave, no correlation (discernible from noise) can be observed for any component of $R_{\alpha,\beta}$. The lower noise levels downstream of the shock wave can be attributed to the higher density there such that more particle pairs fall into each δx–δr bin of the histogram. The density ratio is roughly 2 such that the number of molecule *pairs* quadruples. The noise is thus cut in half.

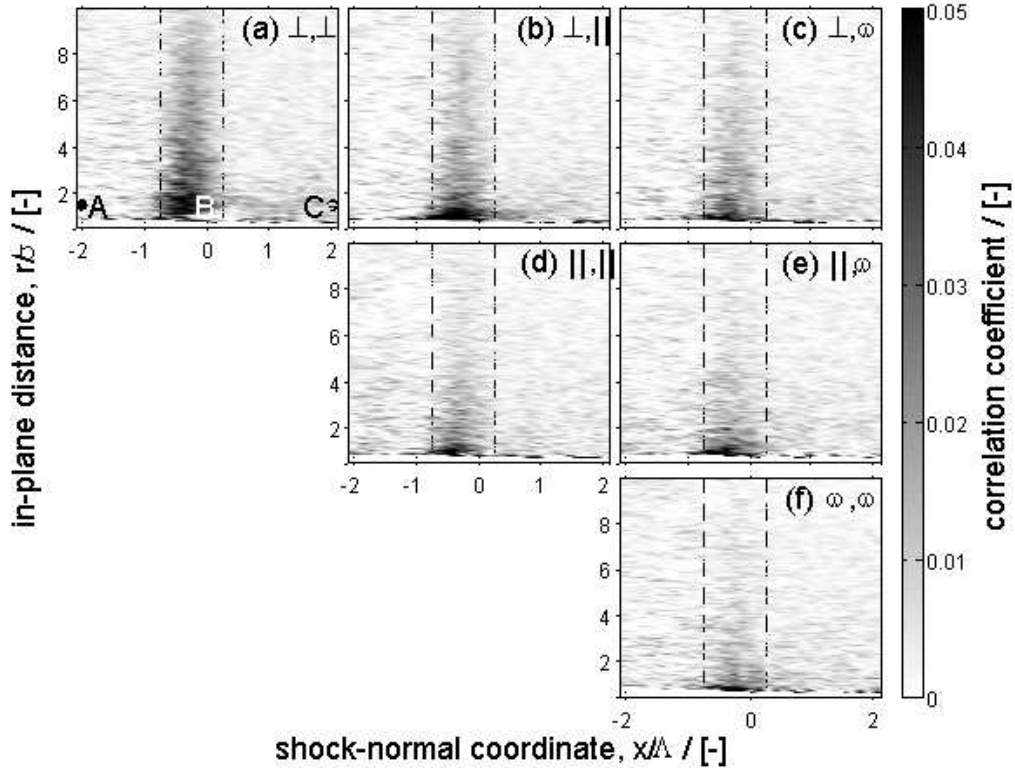

Figure 4: Two–point velocity correlation functions (Eq. 8) within a shock in dense nitrogen. The shock–normal coordinate (horizontal scale) is nondimensionalized by the shock thickness Λ. The vertical scale is the in–plane distance between two molecules within the same slice of thickness $\Delta x = 1$ $\mathring{A}$. It is normalized by the Lennard–Jones radius σ; a): $R_{\perp,\perp}$ b): $R_{\perp,||}$ c): $R_{\perp,\omega}$ d) $R_{||,||}$ e) $R_{||,\omega}$ f) $R_{\omega,\omega}$.

.

The most significant features of Fig. 4 are the long–range positive correlations visible in each panel. They are centered slightly on the cold side of the shock wave. The vertical dashed lines are plotted at $x/\Lambda = -0.75$ and $x/\Lambda = 0.25$ as visual aids. The two–point correlation between the shock–normal velocity is strongest (Fig. 4a), but still weak in absolute terms, reaching only ~ 0.05 for small r. $R_{\perp,\perp} > 0$ is clearly distinguishable from noise for $r/\sigma = 10$ ($\sim 6\times$ pre–shock mean distance between molecules). The other components of R deviate less from zero. But since the correlations exist for all components of R, it is probably more appropriate to speak of long–range correlations of the molecular kinetic energy. Simulations for a shock wave in dense argon give similar results.

7 Three–dimensional structure of a plane shock wave

Lastly, we want to use the wealth of information, which a molecular dynamics simulation provides to partially re–interpret the shock thickness. The term "shock structure" usually refers to the variation of the various thermodynamic state variables along the shock–normal direction. When measuring, simulating, or theoretically considering the shock structure, data is either averaged along the direction parallel to the shock wave, or it is implicitly assumed that the shock structure is one–dimensional, i.e., that a plane shock wave is truly plane.

Suppose that the shock wave is not plane on microscopic scales. Then, in a Gedankenexperiment, the averaged shock structure can be decomposed into two parts: First, the shock structure one would obtain if the shock wave was indeed truly plane (Fig. 5a). In this case, the local shock structure would be identical to the averaged shock structure everywhere. Second, a broadening effect due to deflections up– or downstream of the shock location from its mean. Consider, for example, the (purely theoretical) case where the shock is a discontinuity locally, but that the plane connecting these discontinuities is wavy (Fig. 5b). Spatial averaging along the in–plane directions would then produce a smooth shock profile with a thickness governed by the amplitude of the plane's deflections. These two limiting cases are shown in Fig. 5(a) & (b), respectively. The averaged profile (shown at the bottom of Fig. 5) could be identical, even though the local profiles (e.g. a step function in Fig. 5b)

are qualitatively different. In our Gedankenexperiment, the averaged shock structure is a superposition of these two cases. Fig. 5(c) & (d) shows two limiting cases with respect to the co–movement of different iso–lines. While the local shock structure is the same everywhere in Fig. 5(c) (yet different from the macroscopic structure), even the local structure varies spatially in Fig. 5(d).

We determine the local density and velocity shock locations $x_{s,\rho}$ and $x_{s,u}$ by finding the location x for given y and z, where the density and the mean velocity within a spherical neighborhood of radius $R = 20\ \mathring{A}$ is the mean between the pre– and the post–shock state. Root [49] uses a somewhat more refined spatial averaging procedure to find the turbulent (on a microscopic level) velocity field behind a chemically reacting shock wave.

We find local shock deflections comparable to the mean–free path. The velocity shock is smoother than the density shock and there is no significant correlation between these deflections. In order to quantify the effect of the three–dimensional structure on the overall shock structure, consider the limiting case shown in Fig. 5(b). Assume that the local shock structure is discontinuous at the local shock location x_s. Then, the cumulative distribution function (CDF) for x_s would be the corresponding averaged shock structure. This is shown in Fig. 6. The solid line and the dotted line are the actual averaged profiles for the density and the velocity across the shock, respectively (as shown in Fig. 1). The velocity shock leads the density shock. The dashed curves are the CDFs for $x_{s,\rho}$ and $x_{s,u}$ (the latter leading the former). Based on these curves, a shock thickness Λ_{CDF} can be calculated for this hypothetical case: Λ_{CDF} represents 71% (density) and 46% (velocity) of Λ. One could say that half or more of the macroscopic shock thickness can be explained by the three–dimensional structure of the shock wave.

The three–dimensional structure is a necessary consequence of the breakdown of the continuum hypothesis on the length scale of the shock thickness. On this microscopic level, the shock is no longer propagating into a homogeneous medium, but into one with local fluctuations of the density, velocity, and temperature. The local speed of propagation for the shock wave will hence vary spatially. The shock remains mostly planar for two reasons: through information exchange in the in–plane directions (molecules have velocity components not just in the shock–normal direction) and because the density, velocity, and temperature average out to their macroscopic values along each shock–normal trajectory.

The re–interpretation of the shock thickness to be partially due to a

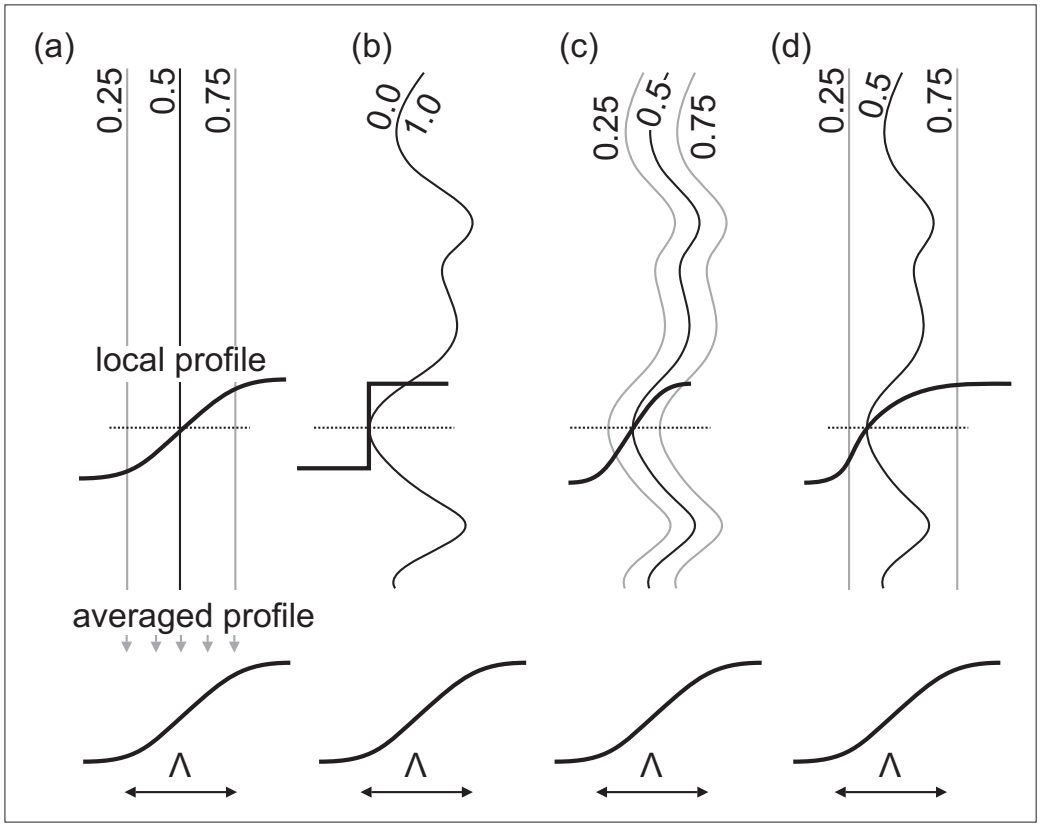

Figure 5: Schematic of some limiting cases for the three–dimensional shock wave structure; (a) truly plane shock wave; (b) wavy discontinuity; (c) strong correlations between iso–density planes; The local shock structure is the same everywhere, but shifted up– or downstream. (d) no correlation between iso–density planes.

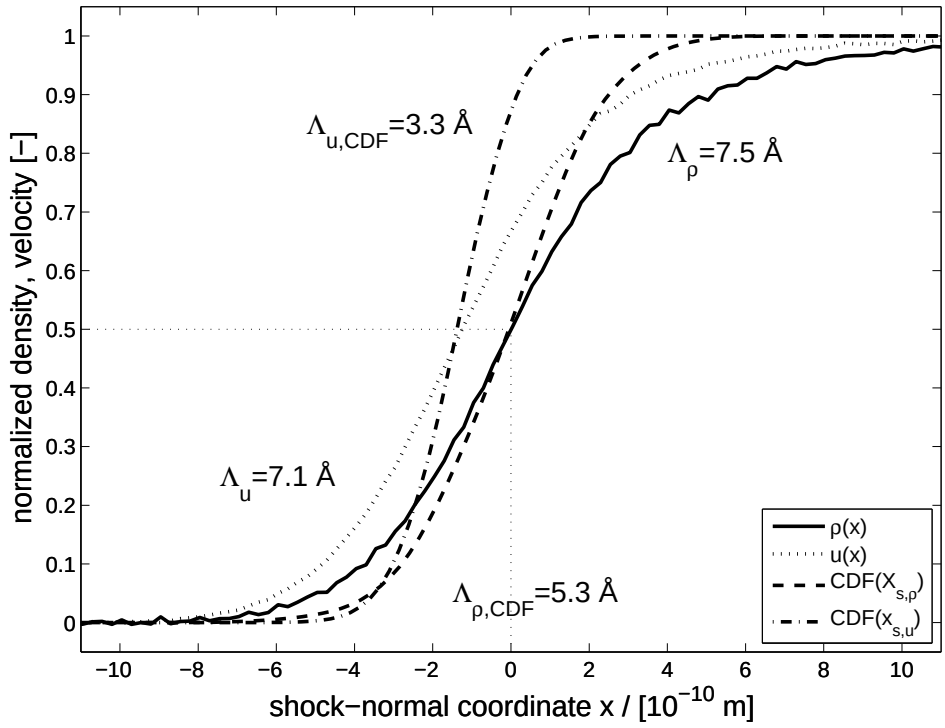

Figure 6: Density and velocity profiles across shock wave in nitrogen; solid line: actual structure of density shock; dashed line: cumulative distribution function for $x_{s,\rho}$; dotted line: actual structure of velocity shock; dash–dotted line: cumulative distribution function for $x_{s,u}$.

"surface roughness" of the shock wave might be considered merely semantics, but we believe that this point of view provides an interesting and intuitive alternate interpretation.

As one approaches molecular length scales, the local density, velocity etc. will inevitably fluctuate because of the finite number of molecules within the sample volume. The local shock location will thus show purely statistical fluctuations and we want to determine if the actual fluctuations exceed this level.

To this effect we first want to find characteristic length scales for the purely statistical deflections from scaling arguments. First, consider the deviation of the local density shock location from its mean. Let n_0 be the particle density at $x = 0$ and R be the radius of the neighborhood. Neglecting the particular structure of the radial distribution function (basically the likelihood of finding a molecule at a certain distance) and the non–unity asymmetry factor (Eq. 3) there will be in average $N = \frac{4}{3}\pi R^3 n_0$ particles within the neighborhood of volume $V = \frac{4}{3}\pi R^3$.

Let the standard deviation of N be $\sigma_N \sim 1/\sqrt{N}$. This uncertainty can be converted into a length scale using the local (number) density gradient,

$$\sigma_{x,\rho} \sim \sigma_N \left(\left. \frac{\partial N}{\partial x} \right|_{x=0} \right)^{-1} = \sigma_N \left(V \left. \frac{\partial n}{\partial x} \right|_{x=0} \right)^{-1}. \tag{9}$$

The shock thickness is defined based on the maximum density gradient,

$$\Lambda_\rho \equiv \frac{\rho_2 - \rho_1}{\partial\rho/\partial x|_{max}} = \frac{n_2 - n_1}{\partial n/\partial x|_{max}} = \frac{\Delta n}{\partial n/\partial x|_{max}} \approx \frac{\Delta n}{\partial n/\partial x|_{x=0}}. \tag{10}$$

The last step utilizes the empirical fact that the location of the maximum density gradient is close to the origin and that the gradient at the origin will be comparable to the maximum gradient. Now substitute Eq. 10 into Eq. 9 to find

$$\frac{\sigma_{x,\rho}}{\Lambda_\rho} \sim \frac{\sigma_N}{V\Delta n}, \tag{11}$$

and thus

$$\frac{\sigma_{x,\rho}}{\Lambda_\rho} \sim \left(R^3 n_0\right)^{-3/2} \left(\frac{\Delta n}{n_0}\right)^{-1}. \tag{12}$$

This is the scaling of the statistical shock deflections relative to the shock thickness with changes of the neighborhood radius, the number density at the origin and the density change across the shock.

Consider a few limiting cases. For $R \to \infty$, the deflections vanish as one recaptures macroscopic behavior. For an infinitely weak shock, i.e., $\Delta n \to 0$, the deflections tend to infinity even compared to the shock thickness, which itself tends to infinity in this limit. This is because the microscopic fluctuations exceed the very weak density change across the shock. Now assume that the relative density jump across the shock $\Delta n/n$ remains constant, then an increasing absolute density decreases the relative fluctuations.

For the velocity shock, a similar approach can be taken. The uncertainty of the molecular velocity of each particle within the neighborhood scales with the speed of sound c. Since there are N particles, the uncertainty for the average velocity is $\sigma_u \sim c/\sqrt{N}$. This can be converted into a length scale using the local velocity gradient,

$$\sigma_{x,u} \sim \frac{\sigma_u}{\partial u/\partial x|_{x=0}}. \tag{13}$$

Following the same arguments as above, this can be rewritten as

$$\frac{\sigma_{x,u}}{\Lambda_u} \sim \frac{\sigma_u}{u_0} \sim \frac{a}{(n_0 R^3)^{1/2}\,\frac{\Delta u}{u_0} u_0} = \frac{1}{M_0}\left(R^3 n_0\right)^{-1/2}\left(\frac{\Delta u}{u_0}\right)^{-1}, \tag{14}$$

where u_0 and M_0 are the local velocity and the local Mach number at $x = 0$, respectively. This result is different from Eq. 12 in that it predicts a weaker dependence on R and in that the Mach number enters directly. Consider two shock waves with identical velocity jumps $\Delta u/u_0$ but with different Mach numbers. The same velocity jump achieved at a smaller Mach number leads to larger uncertainty. This is reasonable because a lower Mach number for a given velocity means that the speed of sound is also higher and thus the uncertainty of the local velocity data is elevated.

Eqs. 12 & 14 predict a faster–than–linear decay of the perturbations with exponents -4.5 for the density shock and -1.5 for the velocity shock. These results can be compared to the actual dependence of the shock deflections vs. the neighborhood radius R. If they show a different scaling, then an additional physical process is likely to be at work. In fact, when a physical phenomenon other than just noise underlies the shock deflections, then one would expect that a) it affects the density and the velocity shock equally, and b) the decay with increasing R would be slower than for purely statistical fluctuations.

Fig. 7 shows the standard deviations $\sigma_{x,\rho}$ and $\sigma_{x,u}$ vs. R in a log–log–plot. The dotted lines represent least–squares power–law fits with exponents

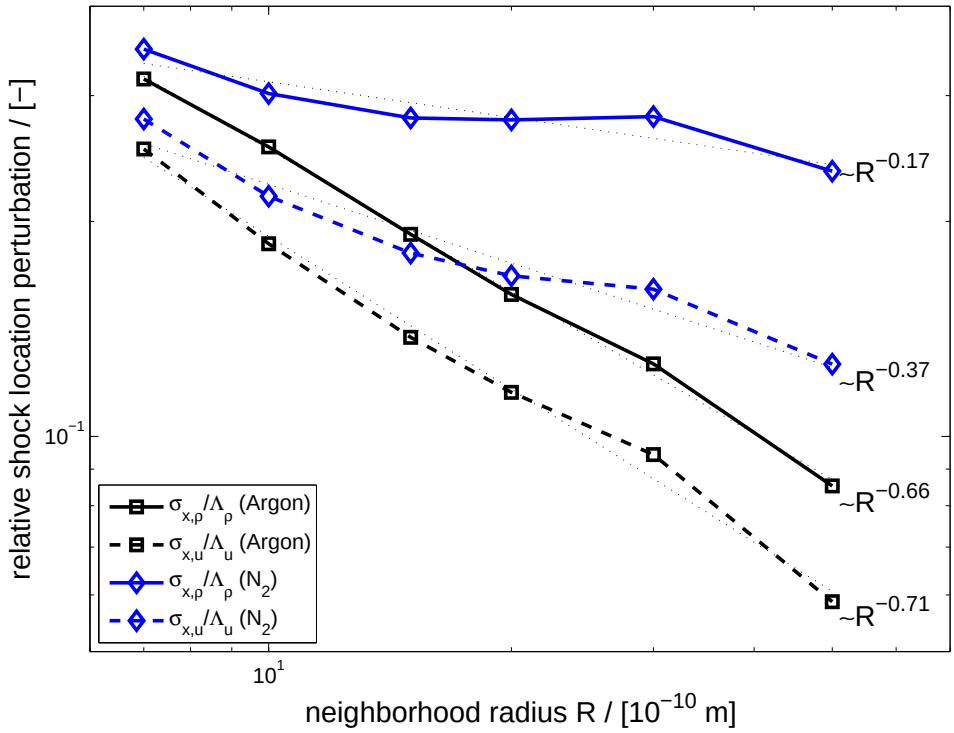

Figure 7: Standard deviation of shock deflections for the density (solid lines) and velocity (dashed lines) shock in argon (black lines) and nitrogen (blue lines) *vs.* neighborhood radius. The dotted lines are power–law fits with exponents as labeled.

as shown in the labels. A few things are worth pointing out: First, the slopes of the lines are much lower than predicted by Eqs. 12 & 14 suggesting that these fluctuations are not just noise. Secondly, the slopes for the density and the velocity shock – while not equal – are comparable and within the uncertainty. Third, and contrary to the predictions in Eqs. 12 & 14, the slopes for the velocity shocks are steeper than for the density shocks. All three features are consistent with and suggest that the fluctuations are not purely noise.

8 Conclusions

The shock structure in dilute and rarefied gases is of engineering interest, because the shock thickness can become comparable (or larger) then some external length scale. In contrast, it is hard to imagine an application where the exact shock structure in a dense fluid can have practical ramifications. The shock thickness there is in the order of a few molecular diameters, and compressible flows are hardly encountered in micro & nano fluid mechanics. Probably the only exception to this rule is the simulation of shock waves in solids, which has military applications.

Shocks in dense liquids thus have to be seen as a benchmark test case either for numerical techniques or for theoretical approaches, because the strong gradients and thermodynamic non–equilibrium effects within them challenge their very foundations. To this end, we have presented a number of phenomena, whose compatibility with other solution techniques can be easily verified? They may also hint at new direction in the theory development.

The effects described owe their discovery to the ever increasing computational resources. The computations require large sample sizes to reveal subtle effects and provide good statistics and had to employ the most expensive (yet most general) computational technique to allow their existence in the first place. But if such measures are taken, then there is still "new physics" left to be discovered even in such a classical problem.

Acknowledgments

This work was sponsored by the Division of Computer Science and Mathematics and used resources of the Center for Computational Sciences at Oak Ridge National Laboratory, which is supported by the Office of Science of the U.S. Department of Energy under Contract No. DE–AC05–00OR22725. Thanks to Mitchio Okumura at the California Institute of Technology for useful discussions.

References

[1] W. V. M. Rankine. On the thermodynamic theory of waves of finite longitudinal disturbance. *Philosophical Transactions of the Royal Society of London*, 160:277–288, 1870.

[2] Rayleigh. Aerial plane waves of finite amplitude. *Proceedings of the Royal Society of London A*, 84(570):247–284, 1910.

[3] G. I. Taylor. The conditions necessary for discontinuous motion in gases. *Proceedings of the Royal Society of London A*, 84(571):371–377, 1910.

[4] G. A. Bird. Approach to translational equilibrium in a rigid sphere gas. *Physics of Fluids*, 6(10):1518–1519, 1963.

[5] G. A. Bird. Shock wave structure in a rigid sphere gas. In J. H. de Leeuw, editor, *Rarefied Gas Dynamics*, volume I, pages 216–222. Academic Press, New York, 1965.

[6] G. A. Bird. Direct simulation and the Boltzmann equation. *Physics of Fluids*, 13(11):2676–2681, 1970.

[7] B. J. Alder and T. E. Wainwright. Phase transition for a hard sphere system. *Journal of Chemical Physics*, 27:1208–1209, 1957.

[8] W. G. Hoover. Structure of shock wave front in a liquid. *Physical Review Letters*, 42(23):1531–1534, 1979.

[9] B. L. Holian, W. G. Hoover, B. Moran, and G. K. Straub. Shock–wave structure via non–equilibrium molecular–dynamics and Navier–Stokes continuum mechanics. *Physical Review A*, 22(6):2798–2808, 1980.

[10] S. Schlamp and B. C. Hathorn. Molecular alignment in a shock wave. *Physics of Fluids*, 18(9):096101, 2006.

[11] S. Schlamp and B. C. Hathorn. Higher moments of the velocity distribution function in dense–gas shocks. *Journal of Computational Physics*, 223(1):305–315, 2007.

[12] S. Schlamp and B. C. Hathorn. Incomplete molecular chaos within dense–fluid shock waves. *Physical Review E*, 76:026314, 2007.

[13] S. Schlamp. *Shock Wave Structure in Dense Argon and Nitrogen – Molecular Dynamics Simulations of Moving Shock Waves*. Habilitation thesis, ETH Zurich, Institute of Fluid Dynamics, Sonneggstr. 3, 8092 Zurich, Switzerland, 2007.

[14] D. H. Tsai and S. F. Trevino. Thermal relaxation in a dense liquid under shock compression. *Physical Review A*, 24(5):2743–2757, 1981.

[15] E. Salomons and M. Mareschal. Usefulness of the Burnett description of strong shock waves. *Physical Review Letters*, 69(2):269–272, 1992.

[16] O. Kum, W. G. Hoover, and C. G. Hoover. Temperature maxima in stable two–dimensional shock waves. *Physical Review E*, 56(1):462–465, 1997.

[17] A. K. Macpherson. Formation of shock waves in a dense gas using a molecular–dynamics type technique. *Journal of Fluid Mechanics*, 45:601–621, 1971.

[18] J. Horowitz, M. Woo, and I. Greber. Molecular dynamics simulation of a piston–driven shock wave. *Physics of Fluids (Gallery of Fluid Motion)*, 7(9):S6, 1995.

[19] M. Woo and I. Greber. Molecular dynamics simulation of piston–driven shock wave in hard sphere gas. *AIAA Journal*, 37(2):215–221, 1999.

[20] T. Tokumasu and Y. Matsumoto. Dynamic molecular collision (DMC) model for rarefied gas flow simulations by the DSMC method. *Physics of Fluids*, 11(7):1907–1920, 1999.

[21] K. Refson. Moldy: A portable molecular dynamics simulation program for serial and parallel computers. *Computer Physics Communications*, 126(3):310–329, 2000.

[22] C. S. Murthy, S. F. O'Shea, and I. R. McDonald. Electrostatic interactions in molecular crystals – lattics dynamics of solid nitrogen and carbon dioxide. *Molecular Physics*, 50(3):531–541, 1983.

[23] M. Linzer and D. F. Hornig. Structure in shock fronts in argon and nitrogen. *Physics of Fluids*, 6(12):1661, 1963.

[24] J. M. Montanero, M. L. de Haro, A. Santos, and V. Garzo. Simple and accurate theory for strong shock waves in a dense hard– sphere fluid. *Physical Review E*, 60(6):7592–7595, 1999.

[25] L. H. Holway. Temperature overshoots in shock waves. *Physics of Fluids*, 8(10):1905–1906, 1965.

[26] S. M. Yen. Temperature overshoot in shock waves. *Physics of Fluids*, 9(7):1417–1418, 1966.

[27] G. C. Pham van Diep, D. A. Erwin, and E. P. Muntz. Nonequilibrium molecular motion in a hypersonic shock wave. *Science*, 245:624–626, 1989.

[28] B. Schmidt. Electron beam density measurements in shock waves in argon. *Journal of Fluid Mechanics*, 39:361–373, 1969.

[29] B. L. Hicks, S. M. Yen, and B. J. Reilly. The internal structure of shock waves. *Journal of Fluid Mechanics*, 53:85–111, 1972.

[30] J. P. Elliott. Validity of Navier–Stokes relation in a shock–wave. *Canadian Journal of Physics*, 53(6):583–586, 1975.

[31] O. Teschke and E. F. de Souza. Water molecule clusters measured at water/air interfaces using atomic force microscopy. *Physical Chemistry Chemical Physics*, 7(22):3856–3865, 2005.

[32] G. L. Gaines. *Insoluble Monolayers at the Liquid–Gas Interfaces*. Interscience, New York, 1966.

[33] M. Li, A. A. Acero, Z. Huang, and S. A. Rice. Formation of an ordered Langmuir monolayer by a non–polar chain molecule. *Nature*, 367(6459):151–153, 1994.

[34] K. A. Dill and P. J. Flory. Molecular organization in micelles and vesicles. *Proceedings of the National Academy of Sciences of the United States of America – Part 1: Physical Sciences*, 78(2):676–680, 1981.

[35] P. J. Collings and M. Hird. *Introduction to Liquid Crystals: Chemistry and Physics*. Taylor & Francis, London, 1997.

[36] C. Cercignani. *The Boltzmann Equation and its Applications*. Springer–Verlag, New York, 1988.

[37] D. J. Evans and E. G. D. Cohen. Probability of second law violations in shearing steady states. *Physical Review Letters*, 71(15):2401–2404, 1993.

[38] M. S. Green. Brownian motion in a gas of noninteracting molecules. *Journal of Chemical Physics*, 19(8):1036–1046, 1951.

[39] M. S. Green. Markoff random processes and the statistical mechanics of time–dependent phenomena. II. Irreversible processes in fluids. *Journal of Chemical Physics*, 22(3):398–413, 1954.

[40] R. Kubo. Statistical–mechanics theory of irreversible processes. 1. General theory and simple applications to magnetic and conduction problems. *Journal of the Physical Society of Japan*, 12(6):570–586, 1957.

[41] M. S. Green. Comment on a paper of Mori on time–correlation expressions for transport properties. *Physical Reviews*, 119(3):829–830, 1960.

[42] E. G. D. Cohen. Kinetic theory of non–equilibrium fluids. *Physica A*, 118(1–3):17–42, 1983.

[43] H. Grad. On the kinetic theory of rarefied gases. *Communications on Pure and Applied Mathematics*, 2(4):331–407, 1949.

[44] S. Tsuge. On the breakdown of the molecular chaos in the presence of translational nonequilibrium. *Physics Letters A*, 36(3):249–250, 1971.

[45] J. Erpenbeck. Shear viscosity of the hard-sphere fluid via nonequilibrium molecular dynamics. *Physical Review Letters*, 52(15):1333–1335, 1984.

[46] J. F. Lutsko. Molecular chaos, pair correlations, and shear–induced ordering of hard spheres. *Physical Review Letters*, 77(11):2225–2228, 1996.

[47] T. Pöschel, N. V. Brilliantov, and T. Schwager. Violation of molecular chaos in dissipative gases. *International Journal of Modern Physics C*, 13(9):1263–1272, 2002.

[48] K. Tamosiunas, L. P. Csernai, V. K. Magas, E. Molnar, and A. Nyiri. Modelling of Boltzmann transport equation for freeze–out. *Journal of Physics G – Nuclear and Particle Physics*, 31(6):S1001–S1004, 2005.

[49] S. Root, R. J. Hardy, and D. R. Swanson. Continuum predictions from molecular dynamics simulations: Shock waves. *Journal of Chemical Physics*, 118(7):3161–3165, 2002.